Published in final edited form as:
Mol Imaging Biol. 2012 February ; 14(1): 25–31. doi:10.1007/s11307-010-0462-2.

Dosimetry of ^{18}F-Labeled Tyrosine Kinase Inhibitor SKI-249380, a Dasatinib-Tracer for PET Imaging

Mark P. S. Dunphy[1], **Pat Zanzonico**[2], **Darren Veach**[3], **Romel Somwar**[4], **Nagavarakishore Pillarsetty**[3], **Jason Lewis**[3,5], and **Steven Larson**[1,5]

[1]Nuclear Medicine Service, Memorial Sloan-Kettering Cancer Center, 1275 York Avenue, Room H-214B, Box 77, New York, NY 10065, US

[2]Department of Medical Physics, Memorial Sloan-Kettering Cancer Center, 1275 York Avenue, Room H-214B, Box 77, New York, NY 10065, USA

[3]Radiochemistry Service, Memorial Sloan-Kettering Cancer Center, 1275 York Avenue, Box 77, Room H-214B, New York, NY 10065, USA

[4]Sloan-Kettering Institute for Cancer Research, Memorial Sloan-Kettering Cancer Center, 1275 York Avenue, Box 77, Room H-214B, New York, NY 10065, USA

[5]Program in Molecular Pharmacology, Memorial Sloan-Kettering Cancer Center, 1275 York Avenue, Room H-214B, Box 77, New York, NY 10065, USA

Abstract

Purpose—To obtain estimates of human normal-organ radiation doses of ^{18}F-SKI-249380, as a prerequisite step towards first-in-human trial. ^{18}F-SKI-249380 is a first-of-its-kind PET tracer for imaging the in vivo pharmacokinetics of dasatinib, an investigational targeted therapy for solid malignancies.

Procedures—Isoflurane-anesthetized mice received tracer dose via tail vein. Organ time-integrated activity coefficients, fractional urinary and hepatobiliary excretion, and total-body clearance kinetics were derived from PET data, with allometric extrapolation to the Standard Man anatomic model and normal-organ-absorbed dose calculations using OLINDA/EXM software.

Results—The human effective dose was 0.031 mSv/MBq. The critical organ was the upper large intestine, with a dose equivalent of 0.25 mSv/MBq. A 190-MBq administered activity of ^{18}F-SKI-249380 is thus predicted to expose an adult human to radiation doses generally comparable to those of routinely used diagnostic radiopharmaceuticals.

Conclusions—Animal-based human dose estimates support first-in-human testing of ^{18}F-SKI-249380.

Keywords

Positron emission tomography; Dasatinib (substance name); Protein-tyrosine kinases [Mesh]; Molecular imaging; SKI-249380

Correspondence to: Mark P. S. Dunphy; dunphym@mskcc.org.

Electronic supplementary material The online version of this article (doi:10.1007/s11307-010-0462-2) contains supplementary material, which is available to authorized users.

Conflicts of Interest. The authors declare they have no conflicts of interest.

Introduction

The tyrosine kinase inhibitor (TKI) dasatinib is now in early-phase clinical trials as a targeted treatment for various malignancies [1–4]. ^{18}F-SKI-249380 is a radio-labeled analog of dasatinib developed for positron emission tomography (PET) [5]. Human normal-organ estimates for ^{18}F-SKI-249380 are required as part of an exploratory investigational new drug application (*e*IND) being submitted to the Food and Drug Administration (FDA) [6]. This article presents the first estimated human dose estimates for ^{18}F-SKI-249380, as derived from animal studies.

Methods

Preparation of ^{18}F-SKI-249380

^{18}F-SKI-249380 was synthesized as previously described [5]. Briefly, ^{18}F-fluoride ion in aqueous solution was transferred to a Reacti-Vial (10 mL) containing 120 μL of 0.25 M potassium carbonate and 15 mg of Kryptofix 2.2.2 (MW=376.5; 40 μM) in 1 mL acetonitrile. Water was removed by azeotropic distillation with CH3CN (3×1 mL) at 100–105°C under a slow stream of argon. The vial was cooled to 0°C and 1,2-dibromoethane (5 μg) in *o*-dichlorobenzene (500 μL) and heated at 105°C for 10 min. The 2-bromo-1- ^{18}F-fluoroethane formed was distilled at 80°C by bubbling a slow stream of argon (~100 mL/min) into another Reacti-vial maintained at −15°C containing a solution of piperazine precursor (6.5 mg; MW=443.95; 14.6 μM), sodium iodide (9 mg; MW=149.89; 60 μM) and cesium carbonate (5 mg; MW=325.82; 15.3 μM) in 250-μL dimethyl formamide and 150-μL acetonitrile. Distillation was performed over 2–3 min during which maximum activity was transferred into the DMF solution. The transferred activity was measured and the vial septum was replaced with a new septa to minimize loss of the volatile 2-bromo-1-^{18}F-fluoroethane during the subsequent reaction. The alkylation was performed by heating the solution at 135°C for 40 min. The reaction mixture was then cooled and diluted with 1.2 mL of 20% acetonitrile in 50-mM sodium acetate/acetic acid buffer (pH ~5.5) and passed through a 13-mm nylon syringe filter (0.25 μm). The crude product was purified using semi-preparative reversed-phase HPLC (Phenomenex Gemini C18, 10×250 mm, 5 μm, flow rate=4 mL/min, solvent A—50 mM sodium acetate/acetic acid buffer, pH ~5.5; solvent B—acetonitrile; A/B gradient 80/20%→80–20%). ^{18}F-SKI-249380 t*R*=15.3 min. The peak was collected and solvent removed under reduced pressure. The radiochemical yield by analytic HPLC averaged ~8% from end of bombardment. The radiochemical purity was >99% and specific activity ~2,500 mCi/μmol.

Animal Model

Animal data for the ^{18}F-SKI-249380 eIND application were collected consistent with FDA guidelines [6], with preclinical testing in a single animal species sufficient for a pilot, or "Phase-0," microdose clinical. Animal studies were performed under a protocol approved by the Institutional Animal care and Use Committee of Memorial Sloan-Kettering Cancer Center (MSKCC). Ten adult mice (Harlan, Inc., Somerville, NJ), five male and five female, of various strains were studied, including severe combined immunodeficient (SCID) mice (*n*=3), athymic nude mice (*n*=4), and immunocompetent mice (FVB-background, *n*=2; C3H/HeJ *n*=1). Six mice were tumor free. Two SCID mice and two athymic nude mice were part of a subsequent experiment and bore human cancer xenografts on each shoulder; the xenografts averaged 10 mm in diameter.

Positron Emission Tomography

Mice were injected via the tail vein with 7.4 MBq (nominal) of ^{18}F-SKI-249380. The injectate was tracer in <100 μL of eluate diluted to 200 μL with normal saline in 8 mice or

modified cyclodextrin (sulfobutyl ether-β-cyclodextrin)-based solution (Captisol®; CyDex Pharmaceuticals, Inc., Lenexa, KS, USA) in the remaining two mice. The actual administered activity (MBq) was calculated as the syringe activity before injection minus the syringe activity after injection; the activities were measured in a dose calibrator (CRC-127R, Capintec Inc, Ramsey, NJ) and were corrected for physical decay to the time of injection. Mice were anesthetized with 2% inhaled isoflurane (Forane®, Baxter Healthcare, Deerfield, IL) in air at a flow rate of 1 L/min in imaging position in the gantry of one of our dedicated small-animal PET system (FOCUS 120 or R4 microPET™ scanner, Concorde Microsystems, Knoxville, TN). The imaging field of view (FOV) included the entire mouse, except for the distal portion of the tail. PET list-mode acquisition was initiated at tracer injection and was continued for 60 min. Acquisition parameters included a 250–750-keV energy window and a 6-ns timing window. Two of the athymic nude mice were imaged again, 2.5-h post-injection for 15 min. Data were sorted into sinograms by Fourier re-binning and PET images reconstructed by iterative algorithm (default manufacturer settings) without attenuation or scatter correction; data were corrected for physical decay to the time of injection.

Organ Time-Integrated Activity Coefficients

Visualization and analyses of PET images were performed using AsiPRO™ software (Concorde Microsystems, Knoxville, TN). Reconstructed images were parameterized as percent of the injected activity per gram (% IA/g) using a system calibration factor measured with a mouse-size phantom composed of a cylinder uniformly filled with an aqueous solution of ^{18}F of known activity concentration (additional information in the Electronic Supplementary Material (Online Resource 1)) The measured activity in the entire PET FOV, a_{FOV}, during the 0–60-min period should represent ~100% of the administered activity, as the FOV included the entire mouse except a portion of the tail distal to the injection site and there was apparently no excretion of activity over the 60-min imaging period. The a_{FOV} was measured using a volume-of-interest (VOI) encompassing the entire FOV. The a_{FOV}-*versus*-time curve was visually inspected and confirmed no activity entered or exited FOV. A study-specific factor, $n_{FOV}=1/a_{FOV}$, normalized the activity in the PET FOV, a_{FOV}, to 100% of the injected activity. The factor n_{FOV}, was applied to time-integrated activity coefficients for each animal to yield the coefficients per unit administered activity. Normal-organ activities were determined by VOI analysis (see Fig. 1 and the Electronic Supplementary Material (Online Resource 2)) and the resulting time-activity data for each organ fit to an exponential function (Office Excel® 2007 Solver plug-in; Microsoft, Seattle, WA), $\sum_{i=1}^{n}[A_o]_i e^{-(\lambda i)bt}$, where $[A_o]_i$ is the zero-time intercept and $(\lambda_i)_b$ is the biological elimination constant of the component *i* of the organ's time-activity function. The zero-time intercept(s) of each exponential function thus fitted was scaled to adjust for the interspecies differences in body mass and fractional organ masses between mice and the Standard Man (organ masses listed in the Electronic Supplementary Material (Online Resource 3)) by first multiplying each intercept value (% IA/g) by the mouse-to-man body-mass ratio and then multiplying by the corresponding standard man-organ masses, as implemented in OLINDA/EXM [7]. The resulting scaled time-activity function for each organ, or source region r_S, was converted from a biological to an effective time-, $(\lambda_i)_b$, with the corresponding effective clearance constant, $(\lambda_i)_e=(\lambda_i)_b+\lambda_p$, where $\lambda_p=0.378$/h is the physical decay constant of ^{18}F. The resulting effective time-activity function was then integrated to yield the time-integrated activity coefficient (in MBq-h), $\tilde{a}(r_S, T_D)$, for source region r_S over integration time $T_D=\infty$ [8]. Each $\tilde{a}(r_S, T_D)$ was multiplied by the animal-specific n_{FOV} value to yield the time-integrated activity coefficient per unit administered activity (in MBq-h/MBq). The $\tilde{a}(_S, T_D)$ values for each mouse were summed to yield the time-integrated activity coefficient per unit administered activity for all organs visualized, N_{organs}. The total time-integrated activity

coefficient per unit administered activity, N_{total}, was 2.64 Mq-h/Mq, where 2.64=1.44×1.83 and 1.83 is the physical half-life of ^{18}F (in h). Subtracting N_{organs} from N_{total} yields the time-integrated activity coefficient per unit administered activity in the remainder of the body, $N_{remainder}$. Organs contributing to N_{organs}, accounted for ~95% of body mass, while $N_{remainder}$ corresponded to >50% of the administered activity in most animals. The remaining ~5% of body mass likely could not account for the remaining nearly 50% of the administered activity. That presumably is accounted for, predominantly, by excreted activity (see Fig. 2), estimated as explained below.

Marked hepatobiliary and lesser urinary excretion of ^{18}F-SKI-249380 were evident from the microPET studies, as indicated by the intense activity in the gut and the kidneys and bladder, respectively. The relative fractions of urinary *versus* hepatobiliary excretion were estimated as follows. On the 0- to 60-min PET image, VOIs were manually drawn to encompass the kidneys and bladder and the abdomen and pelvis, yielding estimates of the relative fractions of administered ^{18}F-SKI-249380 ultimately excreted via the urinary and the hepatobiliary pathways, rf_u and rf_h, respectively:

$$rf_u = A_{kb}/A_{ap} \tag{1}$$

$$rf_h = \left(A_{ap} - A_{kb}\right)/A_{ap} \tag{2}$$

where A_{kb} and A_{ap} are the VOI-derived activities in the bladder and kidneys and the abdomen and pelvis, respectively. Implicit in Eqs. 1 and 2 is that the abdomen and pelvis included the bladder and kidney VOI. The fractions of the administered activity excreted via the urinary bladder, f_u, and via the hepatobiliary tract, f_h, were then calculated as follow:

$$f_u = f_e\, rf_u \tag{3}$$

$$f_h = f_e\, rf_h \tag{4}$$

where f_e is the fraction of administered activity excreted:

$$f_e = N_{remainder}/N_{total} \tag{5}$$

The urinary clearance half-time, $(T_{1/2})_u$, was estimated by fitting a rising monoexponential function to the 0- to 60-min activity time data from a VOI encompassing the urinary bladder. Using the animal-specific values of f_u, f_h, and $(T_{1/2})_u$ and assuming a voiding interval of 4.5 h, the dynamic bladder and ICRP 30 GI models, implemented in OLIND/EXM, yielded the human urinary bladder and gastrointestinal tract $\tilde{a}(r_S, T_D)$ values.

Radiation Dosimetry

The experimentally derived human $\tilde{a}(r_S, T_D)$ values derived for each animal were used as the input for calculation of the normal-organ-absorbed doses and the effective dose, using OLINDA/EXM (v.1, Vanderbilt University, Nashville, TN.) The Standard man anatomic

model was used; this model actually contains both female-specific organs (ovaries and uterus) and male-specific organs (prostate gland and testes) [9].

Statistics

Experimental data was summarized by descriptive statistics, including mean, standard deviation, coefficients of variation, range, and 95% confidence intervals, where appropriate.

Results

Table 1 presents the *in vivo* murine biodistribution data and organ time-integrated activity coefficients for the animals studied; these data are consistent with previously reported data obtained by counting of tissues *ex vivo* [5]. The fractional urinary excretion, f_u, was 3.8±1.8% I.A., with $(T_{1/2})_u$ of 0.29±15 h. The calculated biliary excretion, f_h, was 73.4±5.7% IA. Figure 3 shows the experimental-organ active time data obtained. Table 2 presents the calculated human absorbed doses and effective dose for ^{18}F-SKI-249380.

Discussion

This study provides the first human radiation dose estimates for ^{18}F-SKI-249380. The upper large intestines are predicted to receive the highest absorbed dose, consistent with its marked hepatobiliary excretion. A normal-organ dose limit of 50 mSv has been promulgated by the FDA for radiotracer human-study protocols performed under the auspices of its Radioactive Drug Research Committee (RDRC) program [10]. Although not to be construed as a “safe”-*versus*- “unsafe” limit and not applicable as a regulatory limit to non-RDRC investigations, the 50-mSv figure does provide a benchmark of sorts for specifying an administered activity for initial clinical studies of ^{18}F-SKI-249380. Based upon the dose estimates in Table 2, an administered activity of 190 MBq dose of ^{18}F-SKI-249380 would not be expected to exceed the 50-mSv benchmark dose for any normal organ. At the high specific activity achieved, an injection of 190 MBq of ^{18}F-SKI-249380 would correspond to only several micrograms of this compound. Animal toxicity (No Observable Adverse Effect Level, NOAEL) data [5] indicate that no adverse effects are expected in humans at SKI-249380 doses up to at least ~400 μg.

A number of early-phase trials worldwide are evaluating dasatinib as targeted therapy for solid malignancies resistant to current standard therapies [3,11]. Appropriate patient and dose selection are clearly critical optimizing such trials [12]. Furthermore, the FDA and others have emphasized the need to incorporate assays of pharmaco-kinetics (PK) and pharmacodynamics into early-phase cancer therapy trials to more rigorously characterize the response of patients and their tumors to investigational therapeutics [6,12,13]. Data suggest that threshold tumor concentrations of dasatinib are required to achieve a demonstrable clinical response [1,14,15]. Dasatinib therapy, however, is associated with dose-limiting toxicities [3,16]. Currently, human dasatinib trials are restricted to using plasma PK as a surrogate for tumor drug concentrations [16]. Plasma dasatinib levels might not correlate with tumor exposure, however. Tumors may have poor “avidity” for dasatinib caused by mutations in targeted kinases that inhibit dasatinib binding and/or by overexpression of dasatinib-efflux transporters [15], making lesions resistant to the drug. ^{18}F-SKI-249380 PET imaging could potentially allow non-invasive characterization of dasatinib PK in tumors and organs in individual patients. Such PK data are currently unavailable but could fundamentally change dasatinib trial pharmacometrics and design, including dose–response analyses and patient selection [13,17].

In conclusion, the favorable dosimetry estimates together with previously reported toxicity data support human testing of ^{18}F-SKI-249380in a Phase-0 microdose trial.

Supplementary Material

Refer to Web version on PubMed Central for supplementary material.

Acknowledgments

This research was funded by the National Cancer Institute through a Molecular Imaging Training for Oncology Program grant (R25-CA96945) and an *In Vivo* Cellular and Molecular Imaging Center (ICMIC) grant (P50-CA086438). Technical services provided by the MSKCC Small-Animal Imaging Core Facility were supported in part by an NIH Small-Animal Imaging Research Program (SAIRP) grant (R24 CA83084) and an NIH Center grant (P30 CA08748). The authors gratefully acknowledge the contributions of the MSKCC Radiochemistry/Cyclotron Core Facility; technical assistance by Manda Null, Lars Stelter, and Daniel Shin;discussions with Drs. Elmer Santos, Michelle Bradbury and Oula Penate-Medina; and feedback provided two anonymous reviewers, which significantly improved the quality of this manuscript.

References

1. Luo FR, Barrett Y, Ji P, et al. Dasatinib (BMS-354825) pharmacokinetics correlate with pSRC pharmacodynamics in phase I studies of patients with cancer (CA180002, CA180003). J Clin Oncol. 2006; 24(suppl):3046.
2. U.S. National Institutes of Health. 2010 [11 June 2010]. Available at:http://clinicaltrials.gov/
3. Demetri GD, Lo Russo P, MacPherson IRJ, et al. Phase I dose-escalation and pharmacokinetic study of dasatinib in patients with advanced solid tumors. Clin Cancer Res. 2009; 15:6232–6240. [PubMed: 19789325]
4. Wang L, Christopher LJ, Cui D, et al. Identification of the human enzymes involved in the oxidative metabolism of dasatinib: an effective approach for determining metabolite formation kinetics. Drug Metab Dispos. 2008; 36:1828–1839. [PubMed: 18556438]
5. Veach DR, Namavari M, Pillarsetty N, et al. Synthesis and biological evaluation of a fluorine-18 derivative of dasatinib. J Med Chem. 2007; 50:5853–5857. [PubMed: 17956080]
6. U.S. Food and Drug Administration. Guidance for industry, investigators, and reviewers: exploratory IND studie. 2006
7. Stabin MG, Sparks RB, Crowe E. OLINDA/EXM: the second-generation personal computer software for internal dose assessment in nuclear medicine. J Nucl Med. 2005; 46:1023–1027. [PubMed: 15937315]
8. Bolch WE, Eckerman KF, Sgouros G, Thomas SR. MIRD Pamphlet No. 21: a generalized schema for radiopharmaceutical dosimetry—standardization of Nomenclature. J Nucl Med. 2009; 50:477–484. [PubMed: 19258258]
9. Cristy, M.; Eckerman, K. ORNL/ TM-8381. Oak Ridge National Laboratory; Oak Ridge, TN: 1987. Specific absorbed fractions of energy at various ages from internal photons sources. VII. Adult Male.
10. U.S. Food and Drug Administration. 21 CFR Part 361. Prescription drugs for human use generally recognized as safe and effective and not misbranded: drugs used in research. 2009
11. Wang XD, Reeves K, Luo FR, Xu LA, Lee F, Clark E, Huang F. Identification of candidate predictive and surrogate molecular markers for dasatinib in prostate cancer: rationale for patient selection and efficacy monitoring. Genome Biol. 2007; 8:R255. [PubMed: 18047674]
12. Peck CC, Cross JT. Getting the dose right: facts, a blueprint, and encouragements. Clin Pharmacol Ther. 2007; 82:12–14. [PubMed: 17571068]
13. Workman P, Aboagye EO, Chung YL, et al. Minimally invasive pharmacokinetic and pharmacodynamic technologies in hypothesis-testing clinical trials of innovative therapies. J Natl Cancer Inst. 2006; 98:580–598. [PubMed: 16670384]
14. Hiwase DK, Saunders V, Hewett D, et al. Dasatinib cellular uptake and efflux in chronic myeloid leukemia cells: therapeutic implications. Clin Cancer Res. 2008; 14:3881–3888. [PubMed: 18559609]

15. Luo FR, Yang Z, Camuso A, et al. Dasatinib (BMS-354825) pharmacokinetics and pharmacodynamic biomarkers in animal models predict optimal clinical exposure. Clin Cancer Res. 2006; 12:7180–7186. [PubMed: 17145844]

16. Johnson FM, Agrawal S, Burris H, et al. Phase 1 pharmacokinetic and drug-interaction study of dasatinib in patients with advanced solid tumors. Cancer. 2010; 116:1582–1591. [PubMed: 20108303]

17. National Cancer Institute U.S. National Institutes of Health. A workshop regarding what in-vivo molecular imaging probes are needed to support future translational studies in cancer therapeutics. Paper presented at: Strategies for Imaging Priority Targets; Frankfurt, Germany. 2002.

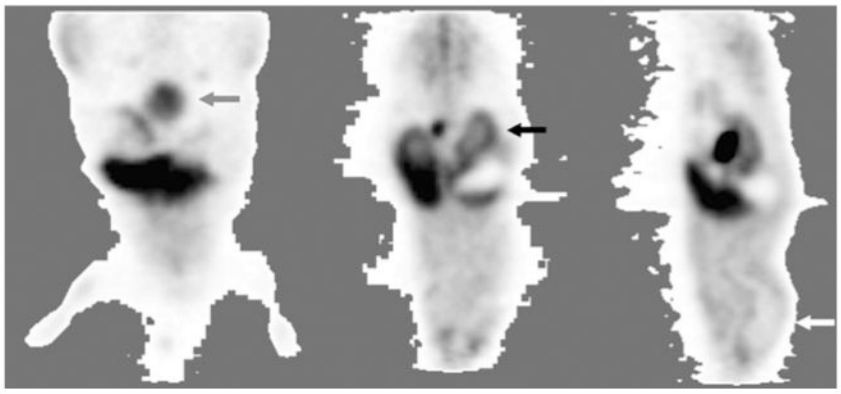

Fig. 1.

Example of animal ^{18}F-SKI-249380 PET imagery for data analyses. In each mouse, 60 min of PET data was reconstructed and summed. Murine organs were selected for special organ-level dosimetric analysis when these demonstrated high or low activity, relative to the remainder of the body, scintigraphically; accounting for all other injected activity, including radioactive excreta, as described in “Methods”. Images: coronal (*left* and *middle*) and sagittal (*right*) sections illustrating, as examples, distinct levels of activity in the urinary bladder (*grey arrow*); renal cortex (*black arrow*); and brain (*white arrow; i.e.*, distinctly low brain uptake—a “deficit” organ). The Electronic Supplementary Material (Online Resource 2) illustrates digital VOI analysis of PET imagery.

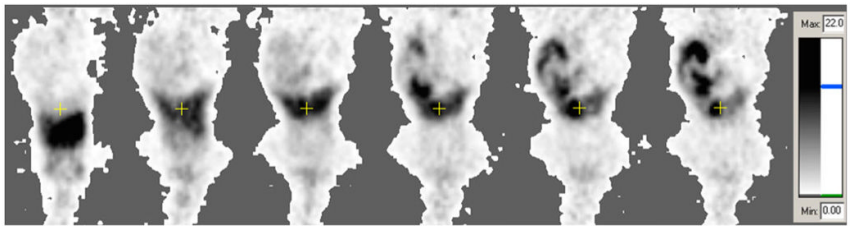

Fig. 2.

Example of animal PET imaging data from one mouse. Shown are serial 1 min-duration frames, of a single coronal plane, obtained during 60 min of dynamic imaging; from left to right: 1, 2, 5, 15, 30, and 60 min, post-tracer injection. The images are scaled to the same grayscale, with black representing ≥22% injected activity/mL. The coronal sections shows the cross-hair centered on the gallbladder region; the head of the mouse is at the bottom of each frame. The images illustrate the predominant hepatobiliary excretion.

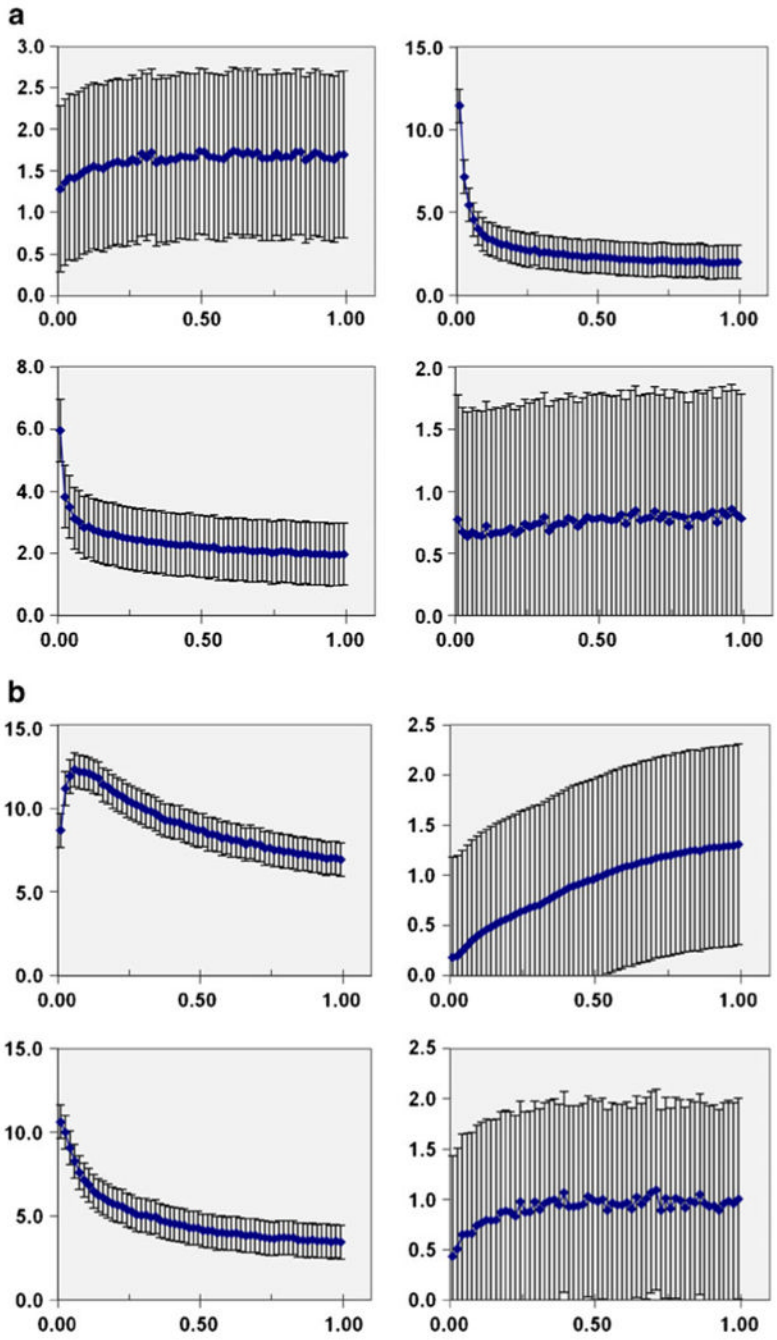

Fig. 3.

Organ activity time data from animal PET imaging. Each datum shown represents the average value from ten mice studied; with *error bars* indicating the standard deviation. Abscissa in units of hours after tracer injection. Ordinate axis in units of % IA/mL; except for urinary bladder data plotted in units of % IA. *Top left:* bone; *top right:* cardiac blood pool; *bottom left:* lungs; *bottom right:* brain. Organ activity time data from animal PET imaging. Each datum shown represents the average value from ten mice studied; with error bars indicating the standard deviation. Abscissa in units of hours after tracer injection. Ordinate axis in units of % IA/mL; except for urinary bladder data plotted in units of % IA.

Top left: liver; *top right:* urinary bladder (excreta); *bottom left:* kidneys; *bottom right:* muscle.

Table 1

Observed ^{18}F-SKI-249380 activity in organs-of-interest at 60 min post-injection and predicted adult human organ time-integrated activity coefficients

Measured activity (% IA)[a]						
Organ	**Average**	**Lowest**	**Highest**	**SD**	**95% CI**	$\tilde{a}(r_S, T_D)$[b]
Bone	9.5	5.1	21.8	4.7	6.2, 12.7	9.2±4.8
Heart contents	0.4	0.2	0.5	0.07	0.3, 0.4	27.7±11.1
Lung	0.5	0.3	1.0	0.2	0.4, 0.6	64.9±33.5
Brain	0.4	0.2	0.7	0.1	0.3, 0.5	44.1±19.3
Liver	7.9	4.7	11.4	1.8	6.6, 9.1	407±163
Kidney	0.8	0.5	1.2	0.3	0.6, 1.0	35.0±17.7
Muscle	26.8	17.0	43.3	8.0	21.3, 32.4	1090±441

[a] Experimentally observed tracer-levels, in units of % injected activity, in organs-of-interest, defined as organs with uptake distinct, scintigraphically, from the remainder of the body, including organs with relatively high-uptake and deficit organs

[b] Predicted adult human organ time-integrated activity coefficient (equivalent to residence time, τ) in units of seconds (average±SD), after allometric interspecies conversion (see “Methods”)

Table 2

Predicted human ^{18}F-SKI-249380 dosimetry

Organ	D[a]	
Adrenals	0.006	
Brain	0.002	
Breasts	0.001	
Gallbladder	0.025	
Lower LI	0.081	
Small intestine	0.221	
Stomach	0.012	
Upper LI	0.252	
Heart wall	0.005	
Kidneys	0.017	
Liver	0.021	
Lungs	0.006	
Muscle	0.008	
Ovaries	0.039	
Pancreas	0.009	
Red marrow	0.010	
Osteogenic cells	0.006	
Skin	0.003	
Spleen	0.007	
Testes	0.003	
Thymus	0.002	
Thyroid	0.001	
Urinary bladder	0.039	
Uterus	0.029	
Total body	0.010	
E[b]		0.031
95% CI, lower limit		0.025
95% CI, upper limit		0.037

LI large intestines

[a] Absorbed dose is expressed in units of mGy/MBq

[b] Effective dose is expressed in units of mSv/MBq